driving seasonal frequency: The maxima of the 12-month running average of the model time series [representing the ENSO warm events (Fig. 1D, upper panel)] occur every 2 to 5 years and always within the same 4 months of the calendar year—precisely the ENSO characteristic missing in the existing simplified delay-oscillator ENSO models. Earlier examinations of ENSO as a low-order chaotic system either have used simplified models lacking the essential equatorial wave dynamics (although they discussed the locking to the seasonal cycle) (13) or did not fully realize the importance of mode locking to the seasonal cycle and the mechanism of resonance overlapping (5).

Is the irregularity of ENSO indeed due to low-order chaos and not to random forcing (2)? The instrumental record of the real ENSO data, which extends over slightly more than 100 years, is too short to identify chaos in an observed time series. Instead, we analyzed the results of the CZ ENSO model (7), which has been used to predict several ENSO events (14).

The diagnostic tool we used to identify chaotic model behavior was the calculation of the phase-space correlation dimension (15) from monthly averaged East Pacific SST from a 1024-year run. The correlation dimension for this run is about $d \approx 3.5$ (Fig. 2A), which suggests a chaotic dynamic system with a small [$\leq (2d + 1)$] number of degrees of freedom.

The correlation dimension calculations are prone to various artifacts (16), and in order to reduce this possibility we used a control time series of surrogate data (17) with the same characteristics (number of points, power spectrum) as the CZ model time series. We chose a time series from a linear Markov model built from the CZ model and driven by random forcing (18). The dimension estimate for the Markov model (Fig. 2B) indicates that this time series is random and distinguishable from the low-order dimension found with the CZ model. This result is consistent with the suggestion that the irregularity of ENSO events (at least in the CZ model) is not due to random noise (such as ocean weather phenomena present in the CZ model).

We suggest that the natural oscillator of the equatorial Pacific ocean-atmosphere system can enter into nonlinear resonance with the seasonal cycle at several periods of the oscillator (mostly 2 to 5 years). The coexistence of these resonances results in chaotic behavior that is due to the jumping of the system among the different resonances. This is a feature of the quasi-periodicity route to chaos (12).

Much additional work is needed to further examine the relevance of these ideas to the observed ENSO characteristics and to clarify the spatial and temporal mechanisms

of the seasonal forcing of Pacific interannual variability. If this theory can be validated, the ENSO cycle might be established as an example of low-order chaos in a highly complex physical system.

REFERENCES AND NOTES

1. M. J. Suarez and P. S. Schopf, J. Atmos. Sci. 45, 3283 (1988).
2. N. E. Graham and W. B. White, Science 240, 1293 (1988).
3. D. S. Battisti and A. C. Hirst, J. Atmos. Sci. 46, 1687 (1989).
4. M. A. Cane, M. Munnich, S. E. Zebiak, ibid. 47, 1562 (1990).
5. M. Munnich, M. A. Cane,.S. E. Zebiak, ibid. 48, 1238 (1991).
6. E. Rasmusson and T. Carpenter, Mon. Weather Rev. 110, 354 (1982).
7. M. A. Cane and S. E. Zebiak, Science 228, 1085 (1985); S. E. Zebiak and M. Cane, Mon. Weather Rev. 115, 2262 (1987).
8. F.-F. Jin, J. D. Neelin, M. Ghil, Science 264, 70 (1994).
9. J. Bjerknes, Mon. Weather Rev. 97, 163 (1969).
10. S. G. Philander, El Niño, La Niña, and the Southern Oscillations (Academic Press, San Diego, CA, 1990).
11. The model parameters are $C_K = L/(2.3\text{ months})$, $C_R = C_K/3$, $a = 1/(180\text{ days})$, $b = 1/(120\text{ days})$, and $c = 1/(138\text{ days})$. Unless indicated otherwise, $A(h)$ is as in (5) with $a_+ = 1$, $a_- = 1$, $b_+ = 2.0$, and $b_- = -b_+/5$. Our heuristic model equation produces regular ENSO oscillations when run without the seasonal forcing term. Equation 1 was integrated by use of a high-accuracy, variable-order, variable-step Adams method using routine D02CBF in Fortran Library Manual, Mark II (Numerical Algorithms Group, 1984).
12. P. Bak, T. Bohr, M. H. Jensen, Phys. Scr. T9, 50 (1985); T. Bohr, P. Bak, M. H. Jensen, Phys. Rev. A 30, 1970 (1984).
13. G. K. Vallis, Science 232, 243 (1986); J. Geophys. Res. 93C, 13979 (1988).
14. M. A. Cane, S. E. Zebiak, S. C. Dolan, Nature 321, 827 (1986).
15. P. Grassberger and I. Procaccia, Physica D 9, 189 (1983).
16. J.-P. Eckmann and D. Ruelle, ibid. 56, 185 (1992).
17. J. Theiler, B. Galdrikian, A. Longtin, S. Eubank, J. D. Farmer, in Nonlinear Prediction and Modeling, M. Casdagli and S. Eubank, Eds. (Addison Wesley, Redwood City, CA, 1991), pp. 163–188. The number of model data points used to obtain Fig. 2 is sufficient to determine the correlation dimension of the system based on the theoretical limitations given in (16). In contrast, a real ENSO time series of 100 years at most is probably too short for the dimension estimate.
18. M. A. Cane, S. E. Zebiak, Y. Xue, Eds., Proceedings of the Workshop on Decade to Century Time Scales of Natural Climate Variability, Climate Research Committee, National Academy of Sciences, Irvine, CA, 21 to 24 September 1992 (National Academy Press, Washington, DC, in press).
19. A. M. Fraser and H. L. Swinney, Phys. Rev. A 33, 1134 (1986).
20. We thank M. Munnich and Y. Xue for their help. M.A.C. was supported by grant NA16-RC-0432-03 from the National Oceanic and Atmospheric Administration and grant OCE-90-00127 from NSF.

1 July 1993; accepted 31 January 1994

Growth of Continental-Scale Metro-Agro-Plexes, Regional Ozone Pollution, and World Food Production

W. L. Chameides,* P. S. Kasibhatla,† J. Yienger, H. Levy II

Three regions of the northern mid-latitudes, the continental-scale metro-agro-plexes, presently dominate global industrial and agricultural productivity. Although these regions cover only 23 percent of the Earth's continents, they account for most of the world's commercial energy consumption, fertilizer use, food-crop production, and food exports. They also account for more than half of the world's atmospheric nitrogen oxide (NO$_x$) emissions and, as a result, are prone to ground-level ozone (O$_3$) pollution during the summer months. On the basis of a global simulation of atmospheric reactive nitrogen compounds, it is estimated that about 10 to 35 percent of the world's grain production may occur in parts of these regions where ozone pollution may reduce crop yields. Exposure to yield-reducing ozone pollution may triple by 2025 if rising anthropogenic NO$_x$ emissions are not abated.

The unprecedented increase in the standard of living of humanity since the Industrial Revolution can be attributed in part to

W. L. Chameides and P. S. Kasibhatla, School of Earth and Atmospheric Sciences, Georgia Institute of Technology, Atlanta, GA 30332, USA.
J. Yienger and H. Levy II, Geophysical Fluid Dynamics Laboratory, Princeton University, Princeton, NJ 08542, USA.

*To whom correspondence should be addressed.
†Visiting scientist at Geophysical Fluid Dynamics Laboratory, Princeton University, Princeton, NJ 08542, USA.

two factors: the development of high-input–high-yield agriculture, capable of feeding an increasingly urban population, and an urban-industrial infrastructure, heavily dependent on fossil fuels for the production and transport of manufactured goods (1). The correlation between agriculture and fossil fuel burning is most pronounced in three regions of the northern mid-latitudes (Fig. 1): (i) eastern North America (25° to 50°N and 105° to 60°W); (ii) Europe (36° to 70°N and 10°W to 90°E); and (iii)

eastern China and Japan (25° to 45°N and 100° to 146°E). Within each of these regions, intense urban-industrial and agricultural activities tend to cluster together into a single large network, or plexus, of lands affected by human activity. We use here the term continental-scale metro-agro-plexes (CSMAPs) as shorthand for these three regions to characterize their size and intermingling of agricultural and urban-industrial activities.

Although these regions comprise only 23% of the Earth's continents, the three CSMAPs account for about 75% of the world's consumption of commercial energy and fertilizers and about 60% of the world's food crop production and food exports (2–4). They are also major source regions for atmospheric pollutants such as nitrogen oxides (NO_x = NO + NO_2). More than 50% of global NO_x emissions originate in CSMAPs, and within CSMAPs anthropogenic emissions make up more than 75% of this total (Table 1). Anthropogenic emissions arise primarily from the burning of fossil fuels. However, microbial emissions

from fertilized soils are also significant. Our calculations with the Geophysical Fluid Dynamics Laboratory (GFDL) three-dimensional, global chemical transport model (GCTM) suggest that photochemical smog has become ubiquitous in CSMAPs because of these NO_x emissions, and as a result many of the world's most productive agricultural regions are probably exposed to harmful concentrations of ozone (O_3) (5–7).

Photochemical smog refers to the mix of noxious gases and particles produced near the Earth's surface from the photooxidation of VOC (hydrocarbons and other volatile organic compounds) and CO in the presence of NO_x (8). Although photochemical smog produces several phytotoxins, we focus here on O_3, a component of smog whose effects on vegetation have been well documented (9–12). Concentrations of O_3 tend to be highest in and around urban areas. However, suburban sprawl, growing numbers of automobiles and expanding roadway networks, as well as an increasing reliance on nitrogenous fertilizers, has

greatly increased the spatial scale of photochemical smog in the CSMAPs. Regional O_3 pollution, often associated with summertime high-pressure systems, can extend over thousands of kilometers and encompass agricultural as well as urban areas (13). The repetition of episodes of O_3 pollution over a growing season produces a pattern of chronic exposure that ultimately reduces crop yields.

The specific relation between O_3 dosage and crop yield is complex and depends on several parameters, such as the species and developmental stage of the crop, the environmental conditions, and the pattern and duration of O_3 exposure (10, 11). In general, crop yield reductions of 5 to 10% result when O_3 reaches some threshold concentration, and these reductions increase as the O_3 concentration increases above the threshold. For cumulative exposures over a growing season, the threshold ranges from ~50 parts per billion by volume (ppbv) for sensitive crops, such as several types of winter wheat, to 70 ppbv for insensitive crops, such as rice (6, 11).
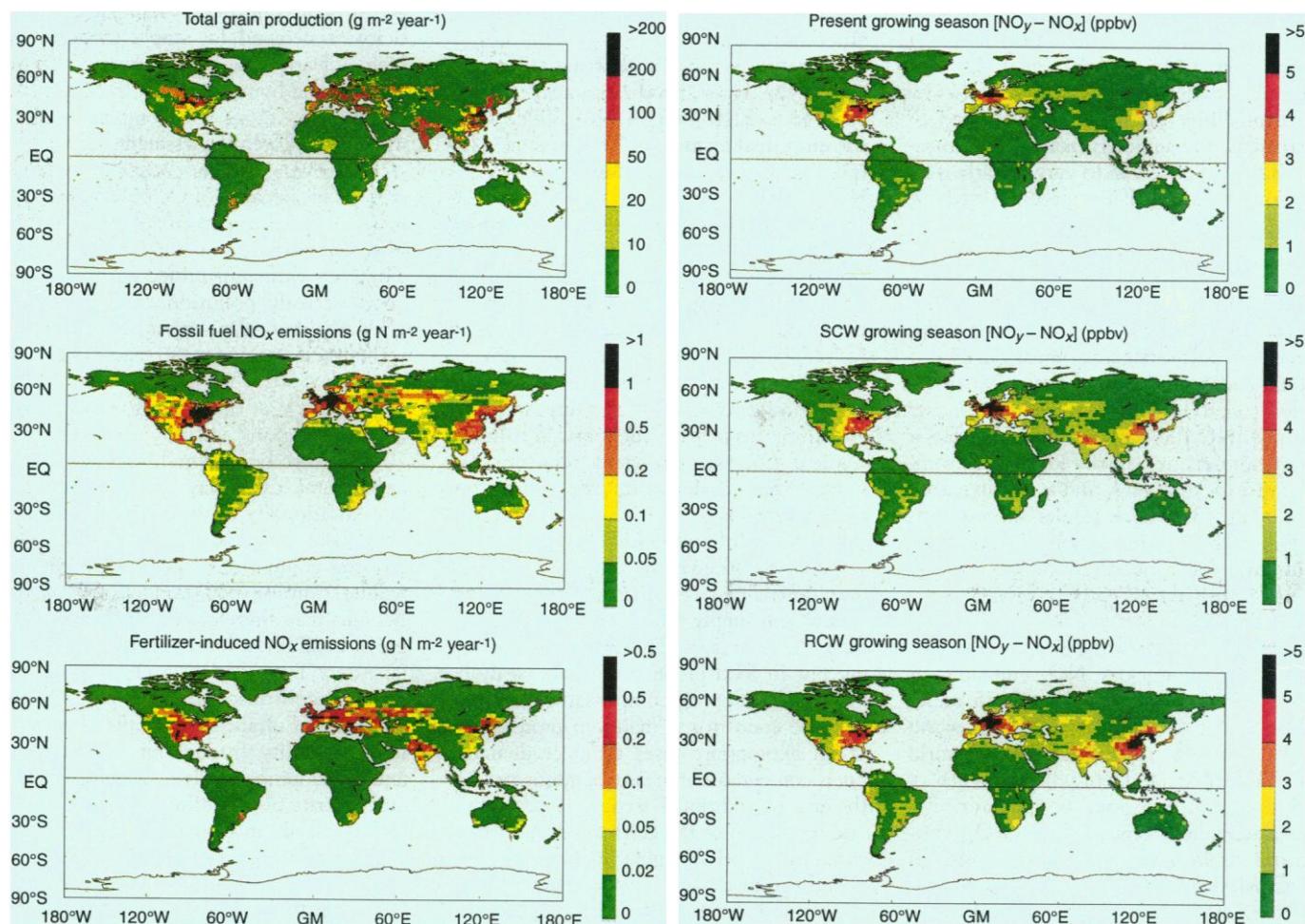
Fig. 1. Geographic distributions of cereal crop production (28, 29, 32, 33), NO_x emissions from fossil fuel burning for the mid-1980s (16), and fertilizer-induced soil emissions of NO_x for the late 1980s (30, 31, 34). GM, Greenwich meridian; EQ, equator.

Fig. 2. Growing season (24) average surface [NO_y – NO_x] calculated by the model with NO_x emissions for the present and for 2025 for slowly changing world (SCW) and rapidly changing world (RCW) scenarios.

Table 1. Emission rates for NO_x (kilotons of N per day) during the growing season (24). Estimates are given for the present (P) and for 2025 assuming slowly changing world (SCW) and rapidly changing world (RCW) scenarios (that is, scenarios with modest and rapid expansion in the global economy, respectively.) Emissions for 2025 are estimated from regional projections for fossil fuel and N fertilizer usage with an econometric model (35). "Other" refers to NO_x emissions sources from natural (nonfertilized) soils (34), biomass burning (36), lightning (17), aircraft (37), and stratospheric N_2O oxidation (38). For sources of fossil fuel emissions and fertilizer-induced soil emissions, see (16, 34).

Source of emissions	Emission rates for CSMAPs in northern mid-latitudes									Global emission rates		
	Eastern North America			Europe			Eastern Asia					
	P	SCW	RCW	P	SCW	RCW	P	SCW	RCW	P	SCW	RCW
Fossil fuels	18	16	18	18	21	25	6.8	13	21	58	77	110
Fertilizer-induced soil emissions	3.6	4.5	4.4	6.4	13	13	1.5	3.1	3.1	15	33	33
Other	3.4	3.4	3.4	4.3	4.3	4.3	2.9	2.9	2.9	40	40	40
Total	25	24	26	29	38	42	11	19	27	113	150	183

Fig. 3. Cumulative percentage of cereal crops grown in areas with a seasonally averaged $[NO_y - NO_x]$ above a given concentration based on model-calculated $[NO_y - NO_x]$ and crop distribution in Fig. 1. Estimates are shown for the present (P), for the present without fertilizer-induced emissions (No fert.), for the present without fossil fuel or fertilizer-induced emissions (No fert., no FF), and for 2025 assuming slowly changing world (SCW) and rapidly changing world (RCW) scenarios. Concentrations of O_3 are from the empirical formula of Trainer et al. (23).

We estimated the areal extent of O_3 pollution and its correlation with agricultural activity from simulations of NO_x and total reactive nitrogen (NO_y) (14) with the GFDL 3D GCTM (15–21). (A dearth of data on air quality on a continental scale precludes a direct determination from O_3 observations.) On regional scales, O_3 production is typically found to be limited by the availability of NO_x (22, 23), and in rural areas, the summertime O_3 concentration has been observed to vary linearly with the concentration of the products of NO_x oxidation (19, 21, 23)—that is,

$$[O_3] = a + b[NO_y - NO_x] \quad (1)$$

where a represents the nominal background O_3 concentration in air not directly influenced by anthropogenic emissions ($\sim$35 ppbv), and b represents the number of O_3 molecules produced for each NO_x molecule emitted into the atmosphere. This latter parameter depends on the local concentrations of VOC and NO_x and generally varies from 5 to 13. These results suggest that $[NO_y - NO_x]$ is a reasonable diagnostic for estimating O_3 concentrations on regional scales.

Figure 2 illustrates the average $[NO_y - NO_x]$ during the growing season (24) calculated for present-day NO_x emissions as well as for those projected for 2025 under scenarios for a slowly changing world (SCW) and a rapidly changing world (RCW) (Table 1). Here, the influence of anthropogenic emissions is apparent. For present-day emissions, $[NO_y - NO_x]$ concentrations in excess of 2 ppbv cluster in the CSMAPs, whereas concentrations outside the CSMAPs generally fall well below 1 ppbv. In the absence of anthropogenic NO_x emissions, we find that $[NO_y - NO_x]$ concentrations in the CSMAPs never exceed 0.5 ppbv, except in northeastern Chi-

na where concentrations approach 1 ppbv. The increase in emissions projected for 2025 intensifies the pollution in the European and Asian CSMAPs and also produces pockets of $[NO_y - NO_x]$ pollution in northern Africa, the Indian subcontinent, and South America.

Our results suggest that a sizable portion of the world's food crops are presently exposed to high $[NO_y - NO_x]$ (Fig. 3). If the empirical formula of Trainer et al. (23) relating O_3 concentration to $[NO_y - NO_x]$ (with a slope of 8.5) were appropriate for all CSMAPs, our calculations would imply that 9 to 35% of the world's cereal crops are presently exposed over the growing season to average O_3 concentrations above the threshold of 50 to 70 ppbv (25). These percentages would drop to 6 to 30%, if there were no emissions from fertilizers, and to 0%, if there were no emissions from fossil fuels and fertilizers. Typical O_3 exposure-yield relations (6) suggest that the losses in crop yields from the current exposure are of the order of a few percent of the world's production of cereals and other crops (26).

Industrialized countries typically restrict agricultural supply through policies to eliminate surplus (27). Thus, a loss of a few percent in food production could easily be made up by adopting compensating measures in these countries to maintain productivity at an appropriate level to meet demand. Such compensating measures might include the use of additional fertilizers, pesticides, and herbicides or the cultivation and irrigation of relatively marginal lands, with associated economic and environmental costs. On the other hand, if such compensating measures are not taken to increase food supply, O_3 pollution could cause an increase in international agricultural prices. Such an increase in prices would likely increase hun-

ger in poor countries, where the price elasticity of demand for staple foods remains high. Clearly, the full economic, environmental, and human costs of the effect of O_3 pollution on crops is a complex issue that will require careful assessment.

Moreover, although the current loss in crop yields because of O_3 pollution appears to be only a few percent of the total, this will likely change in the coming decades. The NO_x emissions projected for 2025 not only intensify pollution over two of the CSMAPs but also enhance pollution in agricultural regions of the developing world. For 2025, we estimate that as much as 30 to 75% of the world's cereals may be grown in regions with O_3 above the 50 to 70 ppbv threshold, which suggests that the agricultural losses may increase significantly. Additionally, this increased pollution effect will be occurring at a time when growing populations in developing nations will be straining food production capacities. Benefits may therefore result from reducing use of fossil fuels, limiting losses of nitrogen fertilizers from soils, implementing NO_x emission controls, and developing O_3-resistant crops. Enhanced networks for monitoring air quality throughout the developed and developing worlds to assess the extent and severity of O_3 pollution on continental scales will aid in evaluating the benefits of these mitigating strategies.

REFERENCES AND NOTES

1. G. D. Ness, in *Population-Environment Dynamics: Ideas and Observations*, G. D. Ness, W. D. Drake, S. R. Brechin, Eds. (Univ. of Michigan Press, Ann Arbor, 1993), pp. 33–56.

2. *Agrostat-PC: Production* (Computerized Information Series, Food and Agriculture Organization, United Nations, Rome, 1991).
3. *1990 Energy Statistics Yearbook* (Bureau of Statistics, United Nations, New York, 1992).
4. *Foreign Trade by Commodities* (Statistics Directorate, Organization for Economic Cooperation and Development, Paris, 1993).
5. Other studies have found significant reductions in crop yields in the United States and in the Kanto district of Japan as a result of O_3 pollution (*6, 7*).
6. R. M. Adams, J. D. Glyer, S. L. Johnson, B. A. McCarl, *J. Air Waste Manag.* **39**, 960 (1989).
7. K. Kobayashi, in *Tropospheric Ozone and the Environment II*, R. L. Bergland, Ed. (Air and Waste Management Association, Pittsburgh, 1992), pp. 537–551.
8. A. J. Haagen-Smit, *Ind. Eng. Chem.* **44**, 1362 (1952); J. H. Seinfeld *et al.*, *Rethinking the Ozone Pollution Problem in Urban and Regional Ozone Pollution* (National Academy Press, Washington, DC, 1991).
9. W. W. Heck, J. A. Dunning, I. J. Hindawi, *Science* **151**, 577 (1966).
10. V. C. Runeckles and B. I. Chevone, in *Surface-Level Ozone Exposures and Their Effects on Vegetation*. A. S. LeFohn. Ed. (Lewis, Chelsea, MI, 1992), pp. 189–270.
11. D. T. Tingey, W. E. Hogsett, E. H. Lee, in *Tropospheric Ozone and the Environment*, R. L. Bergland, D. Lawson, D. McKee, Eds. (Air and Waste Management Association, Pittsburgh, 1989), pp. 272–288.
12. C. A. Ennis, J. Smith, A. L. Lazrus, *Tellus* **45B**, 40 (1993).
13. F. M. Vukovich, W. D. Bach, B. W. Crissman, W. J. King, *Atmos. Environ.* **11**, 967 (1977); R. Guicherit and H. Van Dop, *ibid.*, p. 145; J. A. Logan, *J. Geophys. Res.* **94**, 8511 (1989); J. Fishman, F. M. Vukovich, D. R. Cahoon, M. C. Shipham, *J. Clim. Appl. Meteorol.* **26**, 1638 (1987).
14. NO_y denotes total reactive N and is equal to NO_x plus the N-containing products derived from the oxidation of NO_x.
15. The GFDL GCTM calculates time-dependent distributions of NO_y, NO_x, HNO_3, and peroxyacetyl-nitrate with a simplified photochemical scheme and 12 months of 6-hour wind, temperature, and precipitation fields from a parent global circulation model (*16, 17*). The model has 11 layers in the vertical direction and a horizontal resolution of ~265 km. Table 1 lists the NO_x sources included in our application of the model: the resulting [NO_y – NO_x] values generally agree to within 1σ SD of daytime averaged observations at a number of continental and remote locations (*18–21*).
16. P. S. Kasibhatla, H. Levy II, W. J. Moxim, *J. Geophys. Res.* **98**, 7165 (1993).
17. H. Levy II, W. B. Moxim, P. S. Kasibhatla, in *The Tropospheric Chemistry of O_3 in Polar Regions*, H. Niki and K. H. Becker, Eds. (NATO Advanced Study Institute Series, Springer-Verlag, Berlin, 1993), vol. I7, pp. 77–88.
18. D. D. Parrish *et al.*, *J. Geophys. Res.* **98**, 2927 (1993).
19. T. Wang, thesis, Georgia Institute of Technology, Atlanta (1992).
20. S. T. Sandholm *et al.*, *J. Geophys. Res.* **97**, 16481 (1992); E. L. Atlas *et al.*, *ibid.*, p. 10449.
21. A. Volz-Thomas *et al.*, in *Proceedings of EURO-TRAC Symposium '92*, P. M. Borrell, Ed. (SPB Academic, The Hague, 1993).
22. W. L. Chameides *et al.*, *J. Geophys. Res.* **97**, 6037 (1992); S. Sillman, J. A. Logan, S. C. Wofsy, *ibid.* **95**, 5731 (1990).
23. M. Trainer *et al.*, *ibid.* **98**, 2917 (1993).
24. The growing season is defined as November through February for 90° to 23°S, all year for 23°S to 23°N, and May through August for 23° to 90°N.
25. Virtually identical exposure statistics were calculated with the distribution of all food crops summed together on the basis of their caloric content.
26. This estimate does not account for synergistic effects between O_3 and other pollutants, such as SO_2, or for the fertilizing effects of NO_x deposition. Although the synergistic effects of other pollutants

may cause larger crop reductions than those estimated here (*12*), the latter effect is probably negligible. Application rates of N fertilizers to agricultural plots are generally more than 100 kg of N ha^{-1} $year^{-1}$ (*2*), whereas NO_x emissions from fossil fuel combustion and soil emissions in CSMAPs are 10 kg of N ha^{-1} $year^{-1}$ or less (Table 1).
27. P. Foster, *The World Food Problem* (Lynne Rienner, Boulder, CO, 1992); R. L. Naylor, *Provisioning the Cities into the 21st Century* (Institute for International Studies, Stanford University, Stanford, CA, 1993).
28. *Agricultural Statistics 1992* (U.S. Department of Agriculture, Government Printing Office, Washington, DC, 1992); *World Agricultural Production* (U.S. Department of Agriculture, Circular Series WAP 8-92, Washington, DC, 1992); additional statistics supplied by the Production Estimates and Crop Assessment Division of the U.S. Department of Agriculture, Washington, DC.
29. E. Mathews, *Atlas of Archived Vegetation, Land-Use and Seasonal Albedo Data Sets, NASA Tech. Memo 86199* (Goddard Space Flight Center, Institute for Space Studies, New York, 1985).
30. W. A. Kaplan, S. C. Wofsy, M. Keller, J. M. da Costa, *J. Geophys. Res.* **93**, 1389 (1988); P. S. Bakwin *et al.*, *ibid.* **95**, 16755 (1990).
31. E. J. Williams, A. Guenther, F. C. Fehsenfeld, *ibid.* **97**, 7511 (1992); M. F. Shepard, S. Barzetti, D. R. Hastie, *Atmos. Environ.* **25A**, 1961 (1991).
32. Cereal crops are the total of the production of wheat, rice, and coarse grains such as maize, millet, oats, rye, and barley.
33. Cereal production was derived from country-by-country statistics for 1991 (*2*), except for the United States, Canada, China, and the former Soviet Union, where 1991 statistics at the state or province level were used (*28*). These production statistics were geographically disaggregated onto a 1° by 1° grid with the land use data of Mathews (*29*) renormalized so that the total cultivated area within a given country did not exceed the value reported by the Food and Agriculture Organization (*2*).

34. The NO_x soil source was estimated for 10 generic biomes (water, ice, desert, tundra, scrubland, grassland, woodland, forest, rainforest, and agricultural lands) and geographically distributed with renormalized land use data (*29*). Emissions are assumed to be 0 for water, ice, desert, and scrubland and 3 and 0.5 ng of N per square meter per second for rainforests in the dry and wet seasons, respectively (*30*). Emissions for all other biomes are given by A·exp(0.071T), where T is temperature (in degrees Celsius) and A (nanograms of N per square meter per second) is a fitting parameter for each biome (*31*). For agricultural lands, A is 0.28(F) during the growing season (where F is the fertilization rate in kilograms of N per hectare per month) (*31*) and is equal to that for grasslands during the nongrowing season. The fertilizer-induced soil source is the flux obtained with N fertilization rates reported by the Food and Agriculture Organization (*2*) minus the flux obtained assuming all agricultural lands emit in a manner similar to that of grasslands.
35. D. A. Lashof and D. A. Tirpak, *Policy Options for Stabilizing Global Climate* (Hemisphere, New York, 1990).
36. H. Levy II, W. J. Moxim, P. S. Kasibhatla, J. A. Logan, in *Global Biomass Burning: Atmospheric, Climatic, and Biospheric Implications*, J. S. Levine, Ed. (MIT Press, Cambridge, MA, 1991), pp. 363–369.
37. P. S. Kasibhatla, *Geophys. Res. Lett.* **98**, 1707 (1993).
38. _____, H. Levy II, W. J. Moxim, W. L. Chameides, *J. Geophys. Res.* **96**, 18631 (1991).
39. This research was supported in part by the NSF under grant ATM-9213643 and by the National Oceanic and Atmospheric Administration under grant NA36GP0250. We thank R. Naylor and J. A. Logan for their helpful comments and suggestions, E. Mathews for supplying the global land use data set, and T. Rocke for supplying crop statistics.

Unexpected Square Symmetry Seen by Atomic Force Microscopy in Bilayer Films of Disk-Like Molecules

Nicholas C. Maliszewskyj, Paul A. Heiney,* Jack Y. Josefowicz, John P. McCauley Jr.,† Amos B. Smith III

Thin films of disk-shaped molecules are expected to display anisotropic optical and transport properties, leading to applications in optical display or sensor technologies. Bilayer Langmuir-Blodgett films of monomeric triphenylene mesogens have been studied by atomic force microscopy. The triphenylene cores of the constituent molecules tend to promote the formation of columnar structures in the plane of the substrate and along the direction of deposition of the film. Atomic force microscopy images of bilayer Langmuir-Blodgett films revealed two types of structure, one corresponding to an aligned columnar structure and the other to an unusual square lattice, which may result from the superposition of columnar structures in adjacent layers that intersect at near right angles. Annealing such bilayers near the melting point of the bulk compound improved the structural ordering by reducing the angular spread of orientations associated with the well-developed columnar structure in some areas and by producing a more distinct square lattice in other areas of the sample.

Langmuir-Blodgett (LB) films (*1, 2*) have long been of interest both as model systems for two-dimensional (2D) physics and for their promise in technological applications. Although most research in this area has concentrated on LB films of amphiphilic

rod-like molecules, disk-shaped mesogens exhibiting columnar liquid crystalline phases (*3*) have been shown to form Langmuir (*4*) and LB films (*5, 6*). The electronic conductivity of doped bulk discotic mesophases is highly anisotropic, with most of the conduc-